The high-temperature phase transition in samarium fluoride, SmF_3: structural and vibrational investigation

1998 J. Phys.: Condens. Matter 10 1431

(http://iopscience.iop.org/0953-8984/10/6/026)

J. Phys.: Condens. Matter **10** (1998) 1431–1446. Printed in the UK PII: S0953-8984(98)85126-6

The high-temperature phase transition in samarium fluoride, SmF_3: structural and vibrational investigation

K Rotereau, Ph Daniel†, A Desert and J Y Gesland

Laboratoire de Physique de l'Etat Condensé, UPRES-A No 6087, Université du Maine, avenue Olivier Messiaen, 72085 Le Mans, Cédex 9, France

Received 17 June 1997, in final form 10 November 1997

Abstract. SmF_3 (samarium fluoride) exhibits orthorhombic symmetry (space group *Pnma*; β-YF_3 type) at room temperature and rhombohedral symmetry (space group $P\bar{3}c1$; LaF_3 type) at high temperature. In this paper we describe a study of the structural phase transition mechanism occurring in this compound performed by means of differential thermal analysis, x-ray diffraction and Raman scattering. The transition temperature was determined to be 495 °C and the first-order character of the orthorhombic–rhombohedral phase transition was confirmed. The crystal structure of SmF_3 was refined in the two phases using a Rietveld powder diffraction method. The correlation between the coordination polyhedra appropriate to the two structure types has been established and a proposed transition mechanism is described in this paper. Moreover, a full vibrational investigation of both phases of SmF_3 is presented together with a group theory analysis.

1. Introduction

In the last few years, numerous studies have been devoted to lanthanide fluoride crystals, such as $LiYF_4$ crystal, which is especially well known because of its laser properties. Consequently the ground has been prepared for investigating the potential of yttrium fluoride and the other lanthanide fluorides, LnF_3 (Ln = Sm–Lu), as solid-state laser materials, but the optical properties are strongly dependent on the structural stability of the materials, which is important to be aware of if one is aiming to obtain large crystals with good optical quality. Hence it would appear that it is essential to investigate the mechanism of the structural phase transitions that occur for these compounds, because such transitions could eventually prove destructive of the samples.

These compounds exhibit at room temperature an orthorhombic symmetry with space group *Pnma* (D_{2h}^{16}) with four formula units per unit cell ($Z = 4$), called β-YF_3 type [1, 2]. Among these lanthanide fluorides, only three (SmF_3, EuF_3 and GdF_3) undergo two phase transitions. The first is a first-order phase transition at high temperature (in the range 700 K–1300 K) [1, 3] giving rise to a probable rhombohedral structure (LaF_3 type or tysonite type; space group $P\bar{3}c1$; $Z = 6$ [4–13]). The violent character of this transition is indicated by how difficult it is to grow single crystals directly from the LnF_3 melt, since the samples break when this transition occurs. Some authors [14, 15] report that an additional transition at higher temperature could be detected for these samples close to the melting point, giving rise to a hexagonal structure (Schlyter type; space group $P6_3/mmc$; $Z = 2$ [16]). The

† Author to whom any correspondence should be addressed.

0953-8984/98/061431+16$19.50

compounds LnF_3 (with Ln = Er–Lu and Y) also undergo a first-order phase transition at high temperature (in the range 1200 K–1500 K) [15, 17] to another rhombohedral structure (α-YF_3 type; space group $P\bar{3}m1$; $Z = 1$ [14, 15, 17–19]).

Because the structural transition from the β-YF_3-type structure to the probable LaF_3-type structure generally occurs at high temperature, the mechanism of this phase transformation is still not well known. Among the three compounds SmF_3, EuF_3 and GdF_3, only the first one exhibits a structural phase transition that is relatively easy to observe; this is because it is located at a 'lower' temperature (about 700 K, accessible to experiment) than those for the other isostructural fluorides. Previous authors tried to investigate this phase transition for SmF_3, EuF_3 and GdF_3 [1, 3, 8, 14, 15, 19–25], but their results are very often conflicting because of the difficulty of growing pure crystals. So no answer has been given to the fundamental question for these compounds: what is the exact mechanism of the structural phase transitions occurring for these compounds?

With the aim of answering this question, we report in this paper the results of a differential thermal analysis, x-ray powder diffraction and Raman scattering investigation of SmF_3 between room temperature and 600 °C. A mechanism for the phase transition is proposed that takes into consideration the correlation between the coordination polyhedra appropriate to the β-YF_3 and LaF_3 structure types and structural refinements.

2. Experimental procedure

Single crystals of SmF_3 were grown by slow cooling of the pure melt. Note however that the destructive character of the orthorhombic-to-trigonal first-order structural phase transition that occurs for SmF_3 cannot be avoided as it can for YF_3 [26], and the crystals are systematically broken when the transition occurs. The sample studied by means of Raman scattering was constituted of yellow single-crystal platelets, and this was reduced to powder for the differential thermal analysis and x-ray diffraction experiments.

The differential thermal analysis was carried out on a simultaneous DTA–TGA SDT2960 from TA Instruments, using aluminium oxide as the reference material. Two heating and cooling runs were executed at the rate 10 °C min^{-1}, under an inert argon atmosphere.

The x-ray diffraction data were obtained using a two-circle diffractometer with a Cu tube operating at 40 kV and 30 mA and using a pyrolytic graphite monochromator selecting the Kα lines. Data were collected over a range of 2θ from 20° to 70° at room temperature and from 22° to 60° at high temperature in steps of 0.04°. The high-temperature measurements were realized in a CGR calibrated furnace under a secondary vacuum (10^{-4} mbar). The powder was held back vertically by an aluminium leaf 10 μm thick, so aluminium characteristic diffraction peaks could be observed. Two heating and cooling runs were recorded in order to check the stability of the SmF_3 powder during the experiment. The diffraction patterns were treated with a Rietveld [27] procedure using the Fullprof program [28] for the refinement. The 2θ-region 37°–39° was excluded because of the existence of the intense aluminium line. A Gaussian profile-shape function and a March model for the preferred orientation were chosen. The refined parameters were the diffractometer zero-point error, the three instrumental half-width parameters, the unit-cell dimensions and the atomic positions in the low-temperature symmetry. In the high-temperature phase the atomic positions were calculated but not refined because:

(i) as discussed elsewhere in this paper, a significant proportion of the low-temperature phase is still present at the higher temperatures, which would influence any refinement procedure;

(ii) the number of characteristic peaks of the high-temperature phase observed is small compared with what is predicted by calculations;

(iii) each observed diffraction peak has a weak intensity, especially at high temperature, in spite of a long experimental counting time (from 60 s/point at room temperature up to 95 s/point at 550 °C) selected in order to allow us to clearly distinguish the diffracted lines from the background, which is rather intense at these temperatures; and

(iv) the observed strongly preferred orientation considerably influences the determination of the atomic positions.

Raman spectra were recorded with a Dilor Z-24 triple-monochromator spectrometer equipped with a cooled photomultiplier and coupled to a Coherent argon-ion laser. In the absence of a large SmF_3 crystal, only a back-scattering Raman study without light polarization analysis is possible. In this configuration the scattered light is collected at 180° from the incident laser beam and the investigations are performed under a microscope. The addition of a heating module (a Cheix Meca heating cell) enabled us to record the Raman spectra at high temperature. The spectra were recorded with the wavelength 514.5 nm, the laser power was 700 mW and the spectral width was 6.7 cm^{-1}. A continuous flow of argon was directed at the sample in order to avoid contamination by oxygen from the air.

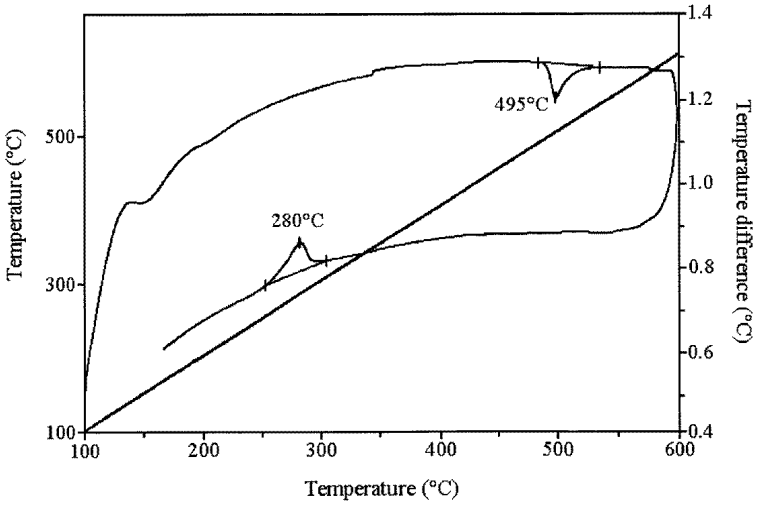

Figure 1. Characteristic DTA thermograms of SmF_3 powder. Second heating and cooling runs are represented.

3. Results

3.1. Differential thermal analysis

Applying differential thermal analysis to SmF_3 allows one to determine rather precisely the temperature of the phase transition for this compound. Two heating and cooling runs were carried out from room temperature up to 600 °C; as is usually observed in DTA experiments on non-calibrated crystal powders, the position of the peak maximum corresponding to the transition can be influenced by the grain size. Consequently the temperature associated with the orthorhombic–hexagonal phase transition was located at 495 °C (see figure 1) during a

second heating run, when the powder could be considered homogeneous. This temperature agrees with the results of Spedding *et al* [22, 23], Greis *et al* [14] and Sobolev *et al* [15], who determined that the transition for pure samples is located at the temperatures 490 °C, 480 °C and 470 °C, respectively. Note that the transition temperatures of compounds contaminated with oxygen are generally higher [3, 20]. During both coolings the hexagonal–orthorhombic peak is situated at only about 280 °C, which shows a very strong hysteresis (∼200 °C).

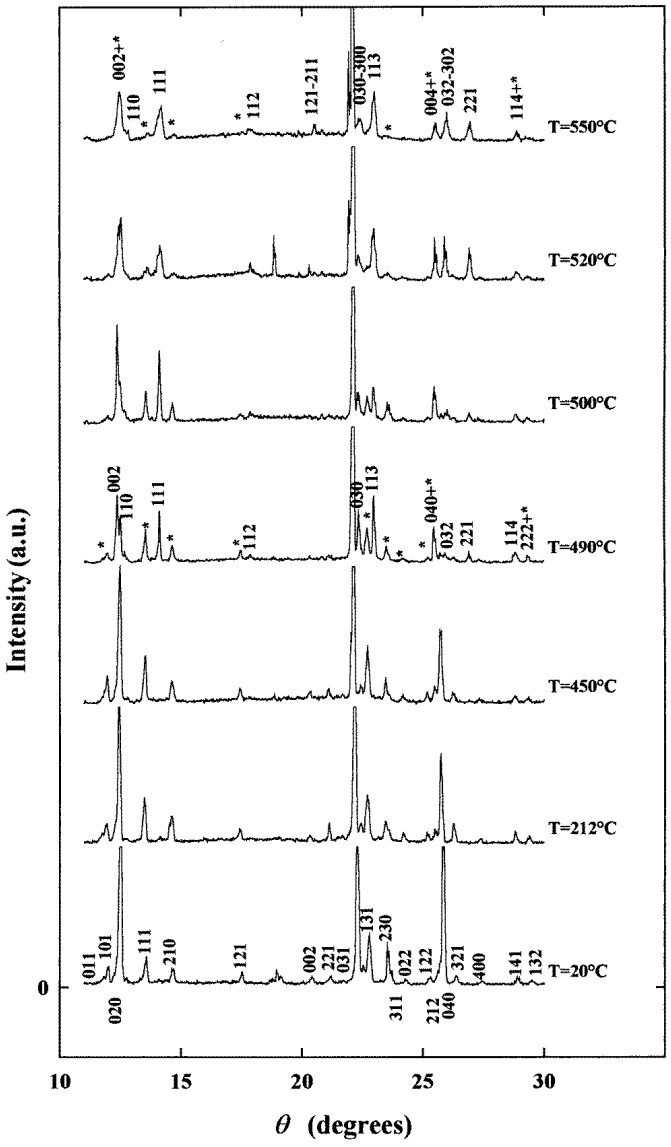

Figure 2. X-ray diffraction patterns of SmF_3 powder between 20 °C and 550 °C. The indexation is with respect to the orthorhombic cell at the lowest temperatures and with respect to the hexagonal cell at the highest temperatures. The asterisks indicate residual diffraction lines from the ambient orthorhombic symmetry.

3.2. X-ray powder diffraction

The diffraction patterns recorded during a heating run between 20 °C and 550 °C are displayed versus temperature in figure 2. As is evident in this figure, a significant modification of the x-ray diffraction patterns measured between 450 °C and 490 °C is observed; it seems incontrovertible that the phase transition occurs in this temperature cycle, which confirms the previous DTA experimental results.

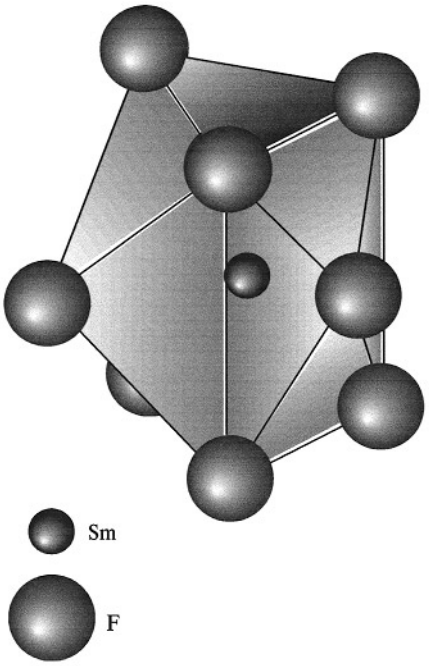

Figure 3. The coordination polyhedron, which is a tricapped prism, constituted of nine fluorine ions surrounding the Sm lanthanide ion in the orthorhombic β-YF_3 symmetry.

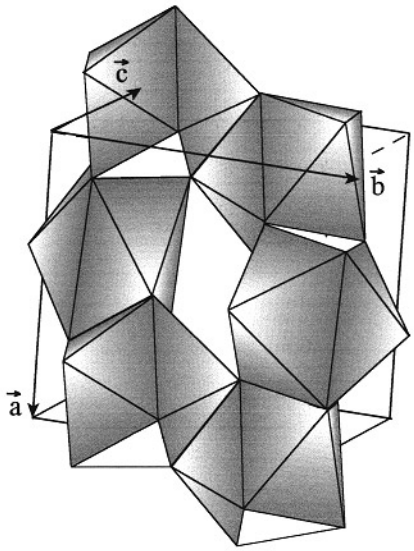

Figure 4. A ring of six tricapped prisms in the orthorhombic β-YF_3 cell.

The Rietveld refinement procedure used for the low-temperature phase confirms the room temperature symmetry previously proposed by different authors [1–3], associated with the orthorhombic *Pnma* space group (D_{2h}^{16}, No 62). Table 1 summarizes the refined parameters, including the cell parameters, atomic positions, scale factors, full widths at half-maximum and parameters describing the preferred orientations, at room temperature, 212 °C and 450 °C. Quality factors are given. The coordination polyhedron previously described in the literature which constitutes the basic unit of the β-YF_3 structure is a tricapped prism with nine fluorine ions surrounding the samarium Sm^{3+} ion. As shown on figure 3, six fluorine ions are at the corners of the irregular trigonal prism with a lanthanide ion at the centre and the three other fluorine ions are in front of the three side faces of this trigonal prism (the fluorine ion located in the background is not represented in figure 2). Except this latter fluorine ion, which is at a greater distance, the fluorine ions are at similar distances from the lanthanide Sm^{3+} ion. The full structure can thus be described by the arrangement, in the orthorhombic cell, of cycles constituted of six tricapped entities, as illustrated in figure 4.

Table 1. Final parameters from the Rietveld refinement for SmF_3 in the orthorhombic β-YF_3 symmetry ($Pnma$, D_{2h}^{16}, No 62) at $T = 20\ ^\circ$C, 212 °C and 450 °C. The reliability factors are the classical quality factors used in powder diffraction refinements (see references [27] and [28]). R_B is the classical Bragg R-factor, R_{wp} the weighted-profile R-factor, and R_{exp} the expected R-factor. W is the full width at half-maximum and G is the refined parameter in the March model for the preferred orientation.

Temperature			20 °C	212 °C	450 °C
Reliability factors	R_B (%)		26.2	17.1	15.2
	R_{wp} (%)		41.6	31.9	32.3
	R_{exp} (%)		12.5	13.2	14.1
Atomic positions	Sm (4c)	x	0.359(2)	0.356(2)	0.357(2)
	$(x, 1/4, z)$	z	0.062(3)	0.063(2)	0.057(2)
	F (4c)	x	0.51(1)	0.52(1)	0.54(1)
	$(x, 1/4, z)$	z	0.55(2)	0.58(2)	0.60(2)
	F′ (8d)	x	0.18(1)	0.14(1)	0.18(1)
	(x, y, z)	y	0.015(5)	0.008(4)	0.010(5)
		z	0.41(1)	0.35(1)	0.40(1)
Cell parameters	a_o (Å)		6.6611(2)	6.673(1)	6.688(2)
	b_o (Å)		7.031(1)	7.050(1)	7.069(1)
	c_o (Å)		4.391(1)	4.403(1)	4.4161(1)
Scale factor	f		34.2×10^{-5} $\pm 0.8 \times 10^{-5}$	37.5×10^{-5} $\pm 0.7 \times 10^{-5}$	33.3×10^{-5} $\pm 0.7 \times 10^{-5}$
Full width at half-maximum	W		0.053(1)	0.056(2)	0.071(2)
Preferred orientation	G (orthorhombic)		0.485(5)	0.601(4)	0.585(4)

At high temperature, for the reasons previously argued, only the cell parameters were refined; the atomic positions were calculated for $T = 550\ ^\circ$C and then these were used for the other temperatures at which the high-symmetry phase is encountered. However, in spite of this approximation, the structure could be satisfactorily solved as is evident from the good reliability factors obtained. In particular, this work confirms unambiguously, for the first time as far as we are aware, that the high-temperature symmetry adopted by SmF_3 is isostructural to the LaF_3 tysonite-type symmetry. The space group adopted is then $P\bar{3}c1$ (D_{3d}^4, No 165), corresponding to a trigonal symmetry usually described in a hexagonal cell. Table 2 summarizes the different structural parameters deduced from our calculations for $T = 490\ ^\circ$C, 500 °C, 520 °C and 550 °C for the hexagonal cell. The samarium ion is now surrounded by an eleven-coordination polyhedron of fluorine ions as shown in figure 5. Each polyhedron is then surrounded by six other similar polyhedra in the hexagonal plane (a_h, b_h) at $z = 1/4$ and $z = 3/4$.

Orthorhombic symmetry is characterized by diffracted lines located at $2\theta = 24.3^\circ$ (101), 25.3° (020), 27.4° (111), 35.3° (121), 41.1° (002), 45.8° (301), 45.9° (131), 48.9° (022), 51.5° (212), 52.0° (040), 53.0° (321) and 58.1° (141), which disappear roughly when the characteristic diffracted peaks of the trigonal structure are observed. These 'hexagonal peaks' are located at $2\theta = 25.0^\circ$ (002), 25.7° (110), 28.6° (111), 36.1° (112), 45.3° (030–300), 46.3° (113), 51.2° (004), 52.4° (032–302), 54.5° (221), and 58.2° (114). A phase coexistence is easy to see; it is characterized by the existence of orthorhombic lines up to

Table 2. Final parameters from the Rietveld refinement for SmF_3 in the trigonal LaF_3 symmetry ($P\bar{3}c1$, D^4_{3d}, No 165) at $T = 490$ °C, 500 °C, 520 °C and 550 °C. (The values given in italics are of non-refined parameters.)

Temperature			490 °C	500 °C	520 °C	550 °C
Reliability factors	R_b (%)		14.9	16.3	16.9	13.2
	R_{wp} (%)		30.3	35.1	41.1	36.4
	R_{exp} (%)		10.9	12.0	10.9	12.8
Atomic positions	Sm	x	*0.66*	*0.66*	*0.66*	*0.66*
	F^I	x^I	*0.39*	*0.39*	*0.39*	*0.39*
		y^I	*0.050*	*0.050*	*0.050*	*0.05*
		z^I	*0.097*	*0.097*	*0.097*	*0.097*
	F^{II}	z^{II}	*0.1369*	*0.136*	*0.1369*	*0.136*
Cell parameters	a_h (Å)		6.990(2)	6.999(2)	7.029(4)	7.011(3)
	c_h (Å)		7.142(2)	7.151(2)	7.176(4)	7.166(4)
Scale factor	f		10.5×10^{-5} $\pm 0.3 \times 10^{-5}$	10.5×10^{-5} $\pm 0.3 \times 10^{-5}$	16.0×10^{-5} $\pm 0.5 \times 10^{-5}$	15.6×10^{-5} $\pm 0.4 \times 10^{-5}$
Full width at half-maximum	W		0.0287(1)	0.0179(9)	0.016(1)	0.012(6)
Preferred orientation	G		0.69(1)	0.66(1)	0.78(2)	0.88(2)

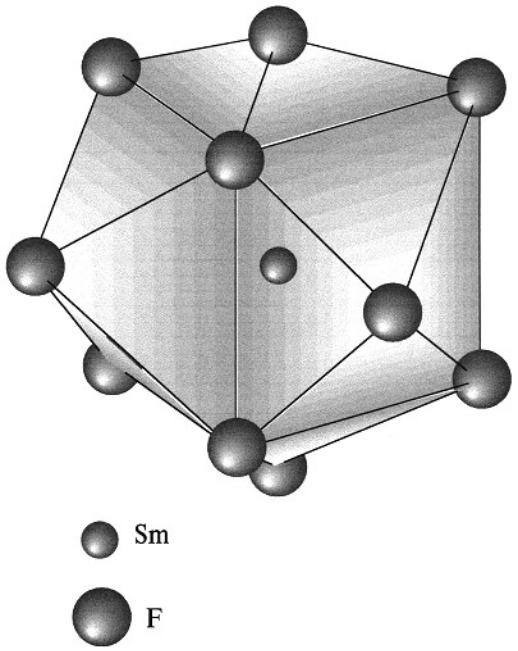

Figure 5. The coordination polyhedron constituted of eleven fluorine ions surrounding the Sm lanthanide ion in the trigonal LaF_3 symmetry (tysonite type).

550 °C together with the persistence of hexagonal weak lines in the diffraction patterns up to room temperature. However, as is shown in figure 6, the proportion of the hexagonal phase in the orthorhombic low-temperature symmetry is low (about 3%) up to 450 °C, which means that the hexagonal phase could be considered as negligible in our refinements up to

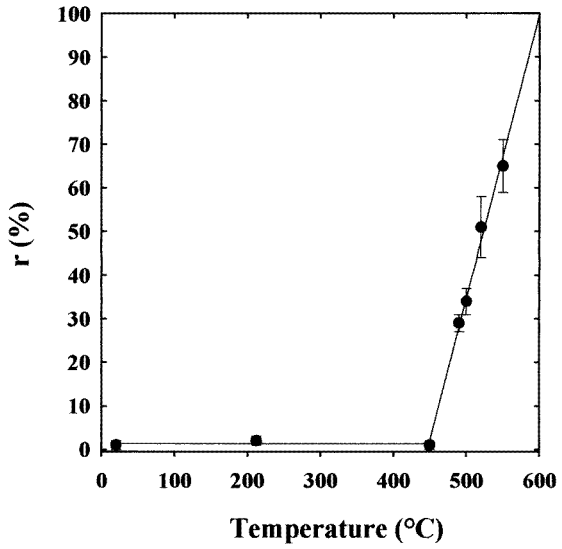

Figure 6. The proportion of hexagonal symmetry domains in SmF_3 versus temperature.

this temperature. On the other hand, above this temperature, the proportion of orthorhombic phase is important, since it corresponds to about 30% of the domains at 550 °C; thus it was necessary to consider the presence of an orthorhombic phase up to this latter temperature, especially in the refinement of the 550 °C x-ray diffraction diagram; this ties in with the difficulty of refining the atomic positions in the trigonal phase.

Furthermore, note that in our Rietveld calculations, in order to take into account the very high intensities observed for the orthorhombic reflections (020) and (040) at room temperature, as compared to the calculated values, a preferred orientation along (010) orthorhombic axes is introduced in this refinement. This hypothesis seems to be consistent with the tricapped-prism arrangement in the β-YF_3-type structure, since these prisms form chains in the direction (010) and the lanthanide ions constitute planes perpendicular to this direction. The same preferred orientation, (001), must be introduced for the hexagonal phase; this is also compatible with the coordination polyhedra arrangement in the LaF_3-type structure, since the lanthanide ions form planes perpendicular to this direction.

3.3. Raman scattering

The recording of the Raman spectra was performed over the temperature range 20 °C–600 °C (see figure 7). Only the usual widening of the lines was observed up to 500 °C during the heating run; above this temperature the spectra become characteristic of hexagonal symmetry. During the cooling run the orthorhombic lines reappear only at 280 °C and they coexist with the hexagonal lines. These Raman measurements confirm the transition temperature and the observation of a strong hysteresis previously noticed by DTA.

Moreover, the vibration modes in SmF_3 have been assigned at room temperature (β-YF_3 type) as well as at high temperature (LaF_3 type). In the orthorhombic symmetry, 24 Raman-active modes are expected:

$$\Gamma_{\text{Raman}} = 7A_g \oplus 5B_{1g} \oplus 7B_{2g} \oplus 5B_{3g}$$

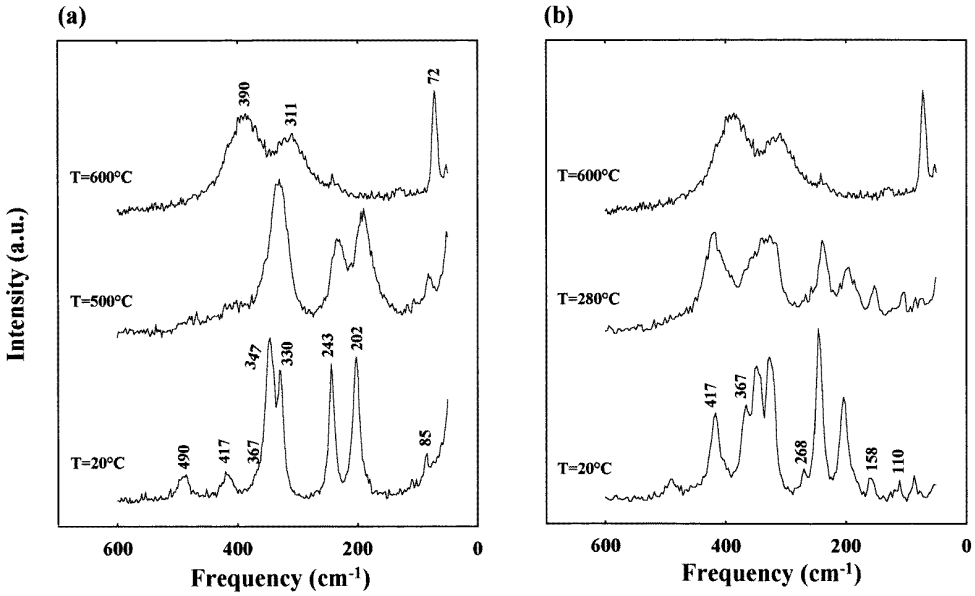

Figure 7. The evolution of the Raman scattering spectra of SmF_3 versus temperature between 20 °C and 600 °C. (a) Heating run. (b) Cooling run.

whereas in the hexagonal phase, 17 Raman-active modes are expected:

$$\Gamma_{\text{Raman}} = 5A_{1g} \oplus 12E_g.$$

Because a large crystal of SmF_3 cannot be grown, analysis of Raman spectra versus selection rules cannot be carried out. So the Raman spectra of SmF_3 at room temperature were assigned by comparison with GdF_3, previously studied by means of Raman scattering [29]. A natural cleavage face appears on the SmF_3 sample, probably corresponding to the [010] orthorhombic crystallographic plane; hence the approximation can be made that the incident and scattered laser beams are parallel to this preferred direction. So the SmF_3 spectrum has to be compared with the GdF_3 spectra in parallel, (aa), (cc), and crossed, (ac), configurations that display the vibration modes A_g and B_{2g}. The more intense lines were then assigned first; so the lines located at 243 cm^{-1}, 347 cm^{-1}, and 202 cm^{-1}, 330 cm^{-1} seem to correspond with the lines located at 244 cm^{-1}, 358 cm^{-1} (A_g modes) and 203 cm^{-1}, 338 cm^{-1} (B_{2g} modes) respectively for the GdF_3 compound. The weak lines at 85 cm^{-1}, 417 cm^{-1}, 490 cm^{-1} can be associated with the lines at 88 cm^{-1}, 429 cm^{-1} (A_g modes) and 501 cm^{-1} (B_{2g} mode). The A_g modes at 110 cm^{-1}, 160 cm^{-1} and 333 cm^{-1} as well as the B_{2g} modes at 93 cm^{-1} and 351 cm^{-1} that were present in the GdF_3 spectra in the three configurations considered are weak or have intense lines superimposed on them, so their equivalent lines cannot be observed in the SmF_3 spectrum. Finally, there is a weak line at 367 cm^{-1} that is to be attributed to a B_{1g} mode, as will be seen below.

The spectrum recorded at room temperature after the cooling run differs a little from the initial spectrum at the same temperature. After the first phase transition, the sample was no longer parallel to the cleavage [010] plane, so the final spectrum could be compared with the GdF_3 spectra in each configuration. Hence the lines at 367 cm^{-1} and 417 cm^{-1} that intensify can be associated with the one at 379 cm^{-1} in the (ba) configuration (a B_{1g} mode) and at 429 cm^{-1} (an A_g mode) respectively for GdF_3. It is probable that the lines

Table 3. Raman-active vibration mode frequencies (cm^{-1}) for SmF_3 at 20 °C compared with those for isostructural compounds at the same temperature (see reference [29]). The values given in italics are not refined, but are simply calculated for orthorhombic symmetry and fixed in this 'hexagonal refinement'.

		SmF_3	GdF_3	TbF_3	YF_3	ErF_3	YbF_3
		(this work)	(reference [29])				
A_g	*1*	**417**	429	434	444	449	455
	2	**347**	358	361	368	373	383
	4	**243**	244	243	245	243	245
	5	**158**	160	163	172	172	175
	6	**110**	110	109	146	108	108
	7	**85**	88	88	120	91	91
B_{1g}	*1*	**367**	379	384	391	395	398
	3	**268**	275	276	295	282	278
B_{2g}	*1*	**490**	501	506	515	520	528
	3	**330**	338	340	350	350	351
	5	**202**	203	197	189	190	175

located at 110 cm^{-1}, 158 cm^{-1} and 268 cm^{-1} correspond to the modes observed for GdF_3 at 110 cm^{-1} (A_g), 160 cm^{-1} (A_g) and 275 cm^{-1} (B_{1g}).

The assignment of the vibration modes for SmF_3 at room temperature is summarized in table 3 and compared there with the attribution obtained for previously studied LnF_3 single crystals (GdF_3, TbF_3, YF_3, ErF_3 and YbF_3) [29]. Eleven vibration modes among the expected 24 Raman-active phonon modes have been assigned for the orthorhombic room temperature phase.

Table 4. Raman-active vibration mode frequencies (cm^{-1}) for SmF_3 at 600 °C compared with phonon frequencies of the LaF_3-type lanthanide fluorides at low temperature (see reference [6]).

		Vibration frequencies (cm^{-1})				
Mode symmetry	Ion involved	LaF_3	CeF_3	PrF_3	NdF_3	**SmF_3**
		(reference [6])				**(this work)**
E_{2g}	Ln^{3+}	79	78	79	81	**72**
E_{2g}	F^-	315	318	321	328	**311**
E_{2g}	F^-	366	388	370	391	**390**

It can be considered that at 600 °C the trigonal symmetry (LaF_3 type) is fully established. So the SmF_3 spectrum at this temperature can be compared with those of LaF_3 and PrF_3 single crystals, which exhibit the same symmetry at room temperature, and of which a Raman study was performed by Bauman and Porto [6] at low temperature. For this high-temperature experiment, the SmF_3 Raman spectrum exhibits three intense broad lines located at 72 cm^{-1}, 311 cm^{-1} and 390 cm^{-1}. This spectrum is similar to that of LaF_3 in the crossed (yx) configuration, which contains three intense lines located at 79 cm^{-1}, 315 cm^{-1} and 366 cm^{-1}, and other lines that cannot be resolved in the SmF_3 spectrum because of the experimental conditions. The spectrum of SmF_3 in the same configuration can also be compared to that of PrF_3, which contains, in addition to the three intense lines at 79 cm^{-1},

321 cm^{-1} and 370 cm^{-1}, a fourth one at 401 cm^{-1}. It follows from the vibrational study carried out by Bauman and Porto [6] for LaF_3 and PrF_3 that the three intense lines of SmF_3 are associated with E_{2g} vibration modes that correspond to a Sm^{3+}- or F^--ion movement in the plane perpendicular to the hexagonal [001] direction. The results of these attributions are summarized in table 4; only three E_{2g} vibration modes among the 12 expected ones have been attributed and no A_{1g} phonon mode has been detected. Note in the SmF_3 spectrum at 600 °C the presence of two orthorhombic lines located at 200 cm^{-1} and 240 cm^{-1} above the transition giving rise to hexagonal symmetry. This remark ties in with the phase coexistence previously observed in x-ray diffraction experiments.

Furthermore, the similarity between the recorded Raman spectra of SmF_3 and the polarized Raman spectra of LaF_3 [6] suggests that the preferred cleavage face of our SmF_3 sample can be associated with a [001] direction in the hexagonal phase. Consequently it seems that the orthorhombic [010] direction becomes the hexagonal [001] direction.

4. Discussion: the mechanism for the β-YF_3-to-LaF_3 structural phase transition

Hence, from these structural and dynamical results, it becomes possible to approach the description of the mechanism of the structural phase transition occurring for the isostructural SmF_3 lanthanides. Firstly, we attempted to establish a correlation between the orthorhombic and hexagonal symmetries in the framework of a group–subgroup relation between the two phases. This rough approximation—especially rough in the case of a first-order phase transition—constitutes a first useful step towards interpreting the transition.

Simply on the basis of geometric considerations, the following cell transformation from hexagonal to orthorhombic symmetry can be proposed:

$$\begin{aligned} \boldsymbol{a}_h &= -\boldsymbol{a}_o \\ \boldsymbol{b}_h &= \frac{1}{2}(\boldsymbol{a}_o + 3\boldsymbol{c}_o) \\ \boldsymbol{c}_h &= \boldsymbol{b}_o \end{aligned} \tag{1}$$

where a_o, b_o, c_o are the orthorhombic cell vectors and a_h, b_h, c_h are the hexagonal cell vectors. From (1) we can easily deduce the following relations between the moduli of the parameters:

$$a_o = a_h \qquad b_o = c_h \qquad c_o = a_h/\sqrt{3}. \tag{2}$$

On introducing in these equations the orthorhombic cell parameters measured in our x-ray diffraction experiments at room temperature, it is easily checked that the predicted hexagonal cell parameters are similar to the ones that we have measured (or the ones given in the literature for LaF_3-type lanthanide fluorides [8, 22, 23]), which confirms the appropriateness of the adopted change. Moreover, with this cell transformation, the hexagonal atomic positions calculated from the orthorhombic atomic positions agree with the atomic positions actually adopted by the fluorine ions in LaF_3-type lanthanide fluorides.

The evolution of the orthorhombic cell parameters between 20 °C and 550 °C (a_o, b_o, c_o) and of the associated hexagonal parameters from 490 °C to 550 °C (a_h, b_h, c_h) is shown in figure 8. The evolution of the orthorhombic cell volume ($V_0 = a_o b_o c_o$) versus temperature is also displayed in this figure (figure 8(d)). The evolution versus temperature of the corresponding pseudo-orthorhombic cell volume of the high-temperature phase ($V_H = a_h^2 c_h/\sqrt{3}$), deduced from equations (2), is also shown in figure 8(d). It can be noticed that a jump in the parameter values is evident close to the transition, with an unusual contraction of the cell volume when the temperature increases ($\Delta V = V_H - V_0 = -7.27$ Å^3).

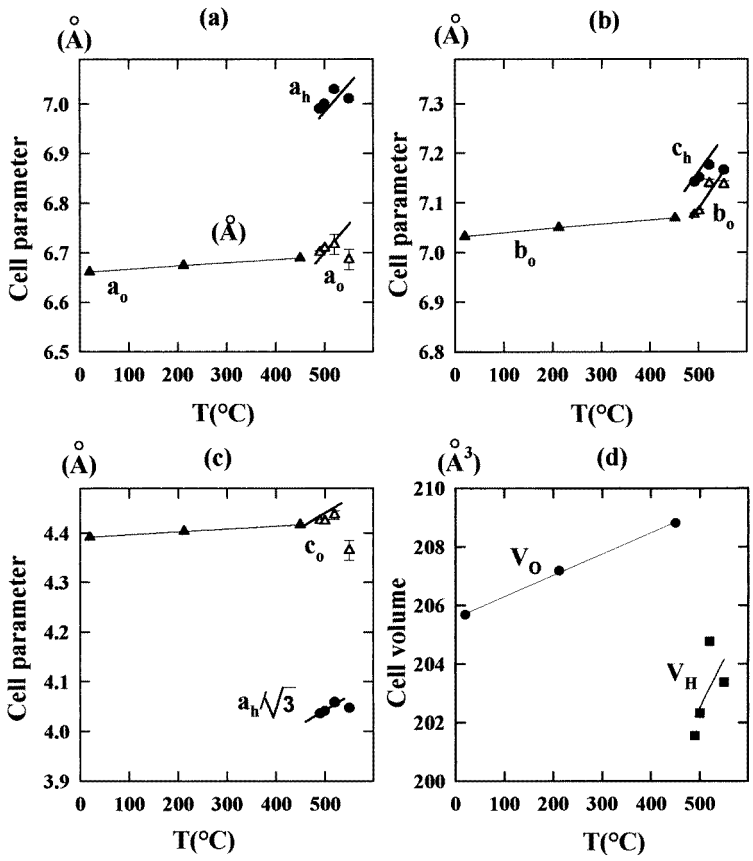

Figure 8. The evolution versus temperature of the orthorhombic (a_o, b_o, c_o) cell parameters, the hexagonal (a_h, b_h, c_h) cell parameters and the cell volume. V_0 is the orthorhombic unit-cell volume. V_H is not the hexagonal cell volume for $P\bar{3}c1$, but the volume deduced from the cell transformation suggested in this paper, i.e. $V_H = a_h^2 c_h/\sqrt{3}$.

This observation is consistent with a first-order destructive transition, and seems to indicate that the high-temperature symmetry is not a stable structure for this kind of sample.

Within the framework of this cell transformation, the conditions limiting the possible reflections in the orthorhombic and hexagonal phases are linked up as follows:

$$h_h = h_o$$
$$k_h = \frac{1}{2}(h_o + 3l_o)$$
$$l_h = k_o.$$

The connections between the real conditions limiting the $(h_o k_o l_o)$ orthorhombic reflections and the deduced conditions limiting the $(h_h k_h l_h)$ hexagonal reflections are reported in table 5. There is no condition for the $(h_h h_h 0)$ and $(h_h h_h l_h)$ reflections calculated from the $(h_o 00)$ and $(h_o k_o 0)$ reflections, as is to be expected within the context of the space group $P\bar{3}c1$. However, additional conditions for the $(h_h 00)$, $(00l_h)$ and $(h_h 0l_h)$ appear: $h_h = 3p$ for the $(h_h 00)$ and $(h_h 0l_h)$ reflections, $l_h = 2q$ for the $(00l_h)$ and $(h_h 0l_h)$ reflections. This latter condition is supported by experimental observations, since the observed $(00l_h)$ reflections are

002 and 004 and the observed $(h_h 0 l_h)$ reflections are 300, 302 and 200. The first condition is verified for the intense reflections such as 300 and 302, but is very difficult to confirm for the very weak reflections like 200. Moreover, the more intense orthorhombic reflections (020, 040, 111 and 210, 131, 230) are connected to intense hexagonal reflections (002, 004, 111, 113) as expected from this cell transformation. Finally, it has been shown by the x-ray diffraction and Raman scattering measurements that the orthorhombic [010] direction becomes the hexagonal [001] direction, which agrees with the proposed cell transformation.

Table 5. The correspondence between the orthorhombic $(h_h k_h l_h)$ reflections and the calculated hexagonal $(h_o k_o l_o)$ reflections.

Conditions limiting the $(h_o k_o l_o)$ orthorhombic reflections		Conditions limiting the $(h_h k_h l_h)$ calculated hexagonal reflections	
$(h_o 00)$	$h_o = 2n$	$(h_h h_h 0)$	$h_h = n$
$(0 k_o 0)$	$k_o = 2n$	$(00 l_h)$	$l_h = 2n$
$(00 l_o)$	$l_o = 2n$	$(h_h 00)$	$h_h = 3n$
$(h_o k_o 0)$	$h_o = 2n$	$(h_h h_h)$	$l_h - h_h = n$
$(0 k_o l_o)$	$k_o + l_o = 2n$	$(h_h 0 l_h)$	$h_h = 3p$, $l_h = 2q$

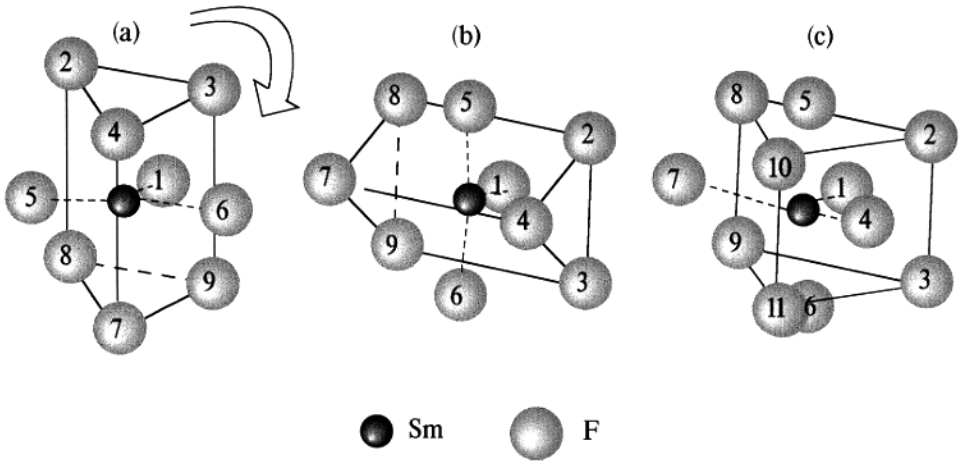

Figure 9. The transformation from the tricapped prism of orthorhombic symmetry (a) to the 11-coordination polyhedron of hexagonal symmetry (c). A representation of the initial tricapped prism in the horizontal position is given in (b).

Because the x-ray diffraction and Raman scattering measurements have enabled us to confirm the proposed cell transformation between the two symmetries, it is now possible to establish the correlation between the coordination polyhedra forming the basis of the β-YF_3 and LaF_3 structural types, and so to describe rather accurately the orthorhombic–hexagonal transition mechanism for the archetype SmF_3 compound. A correspondence between the fluorine ions deduced from the previously referred to cell transformation has been established between the two types of polyhedron, and now a comparison between the polyhedral geometries can be made on the basis of data obtained by means of refinements in the hexagonal and orthorhombic symmetries.

As mentioned previously, the basic forms from which the structure is constituted are

Table 6. Experimental bond lengths and bond angles in SmF_3 at $T = 20$ °C (orthorhombic symmetry) and $T = 550$ °C (hexagonal symmetry). Only the distances between nearest neighbours in a polyhedron are given. The fluorine ions are numbered according to the labelling adopted in figure 9. Distances are given in Å and angles in degrees.

Distances	Orthorhombic phase $T = 20$ °C	Hexagonal phase $T = 550$ °C
Sm–F1	2.43 ± 0.1	2.454 ± 0.03
Sm–F5	2.007 ± 0.04	2.516 ± 0.008
Sm–F6	2.007 ± 0.04	2.516 ± 0.008
Sm–F2	2.757 ± 0.06	2.356 ± 0.06
Sm–F3	2.757 ± 0.04	2.356 ± 0.06
Sm–F4	2.45 ± 0.1	2.454 ± 0.03
Sm–F8	2.514 ± 0.06	2.484 ± 0.03
Sm–F9	2.514 ± 0.06	2.484 ± 0.03
Sm–F7	2.3218 ± 0.1	2.384 ± 0.07
Sm–F10	—	2.945 ± 0.03
Sm–F11	—	2.945 ± 0.03
F2–F8 or F3–F9	3.61 ± 0.1	3.398 ± 0.07
F2–F4	2.87 ± 0.1	2.526 ± 0.007
F8–F7	2.87 ± 0.1	2.484 ± 0.03
F3–F4 or F7–F9	2.87 ± 0.1	—
F2–F3 or F8–F9	3.305 ± 0.05	2.266 ± 0.009
Sm–Sm	3.713 ± 0.02	—
Angles	**Orthorhombic phase $T = 20$ °C**	**Hexagonal phase $T = 550$ °C**
F1–Sm–F5	105.8 ± 4.1	113.4 ± 1.0
F1–Sm–F6	105.8 ± 4.1	62.5 ± 0.5
F5–Sm–F6	148.3 ± 8.0	171.9 ± 3.0
F4–Sm–F1	127.9 ± 3.0	125.6 ± 3.0
F4–Sm–F7	102.45 ± 3.0	117.2 ± 1.0
F1–Sm–F7	102.45 ± 3.0	117.2 ± 1.0

tricapped prisms in the orthorhombic low-temperature phase (see figure 3). In this case, the coordination number associated with the Sm^{3+} ion is 9. It is also now established that in the hexagonal high-temperature symmetry the coordination polyhedron is built up from eleven fluorine ions: nine of them form a similar tricapped prism around the lanthanide ion, and the two remaining fluorine ions are located as follows: one above the upper triangular face and the other one below the opposite triangular face. Each triangular face of the prism supports thus a trigonal pyramid (see figure 5). With the help of the geometrical correspondence between the fluorine-ion positions in the two structures, the transformation undergone by the orthorhombic tricapped prism can be illustrated as shown in figure 9, where each fluorine ion involved is labelled with an appropriate number. A comparison between the experimental bond lengths and bond angles of the two phases, obtained from our refinements, is exhibited in table 6. The numbers labelling the fluorine atoms are those used in figure 9. From these values it can be deduced that the dimensions of the trigonal prism are strongly modified by the transition: in particular, the prism is smaller and wider in the high-temperature symmetry than in the orthorhombic structure. The distances between the samarium and capped ions of the orthorhombic phase also change a lot in the phase transition. However, except the F1–Sm–F6 angle, which is strongly affected by the structural change, the values of the F–Sm–F angles are roughly preserved.

Finally, the evolution of an orthorhombic polyhedron into a hexagonal one can be described as follows: one rectangular face of the initial trigonal prism is preserved in the hexagonal structure coordination polyhedron, and the fluorine ion which is positioned opposite to this face remains at the same place after the phase transition. The foreground side edge in the hexagonal structure polyhedron is built up from two fluorine ions which do not belong to the initial tricapped prism. The fluorine ions that constitute the foreground lateral edge in the orthorhombic structure tricapped prism become the ions in front of the side faces in the hexagonal structure. Finally the fluorine ions that are located in front of the two remaining side faces in the orthorhombic structure tricapped prism become the ions which are located above and below the triangular faces of the basic trigonal prism in the hexagonal structure. It is thus evident from this transformation that the polyhedra which built up the orthorhombic low-temperature phase are entirely broken in the phase transition, to form similar polyhedra but constituted from other ions. So the first-order character of the transition, evident experimentally, is fully explained.

5. Conclusion

The various experiments have enabled us to fix the phase transition temperature at 495 °C, with coexistence of orthorhombic and hexagonal phases over a 50 °C temperature range. A strong hysteresis (∼200 °C) is also observed. These two main features of the transition indicate its first-order character.

On the basis of the comparison of the SmF_3 Raman spectra with the GdF_3 polarized Raman spectra, 11 vibration modes among the expected 24 Raman-active phonon modes (six among the predicted seven A_g modes, three among the five B_{1g} modes and two among the seven B_{2g} modes) have been attributed at room temperature for SmF_3 as being of orthorhombic β-YF_3 type and three vibration modes among the expected 17 Raman-active phonon modes have been attributed at 600 °C for SmF_3 as being of hexagonal LaF_3 type. From these x-ray diffraction and Raman scattering results, it seems now that the first-order high-temperature transformation has been explained for the SmF_3 compound, and so also for the isostructural compounds EuF_3 and GdF_3. It seems thus that in the search for a method of growing an isotype-doped compound, prompted by its prospective laser applications, such a study is essential.

Acknowledgments

We are greatly indebted to Professor M Leblanc for making the DTA measurements, to Professor A Gibaud for advice given during the x-ray diffraction experiment, to Professor A Bulou for fruitful discussions, and to Dr A Jouanneaux for help with the Rietveld refinements. Also, special thanks go to G Ripault for invaluable help with the high-temperature x-ray diffraction measurements.

References

[1] Zalkin A and Templeton D H 1953 *J. Am. Chem. Soc.* **75** 2453
[2] Cheetham A K and Norman N 1974 *Acta Chem. Scand.* A **28** 55
[3] Thoma R E and Brunton G D 1966 *Inorg. Chem.* **5** 1937
[4] Mansmann M 1964 *Z. Anorg. Allg. Chem.* **331** 98
Mansmann M 1965 *Z. Kristallogr.* **122** 375
[5] Zalkin A, Templeton D H and Hopkins T E 1966 *Inorg. Chem.* **5** 1466

[6] Bauman R P and Porto S P S 1967 *Phys. Rev.* **161** 842
[7] Andersson L O and Johansson G 1968 *Z. Kristallogr.* **127** 386
[8] Greis O and Petzel T 1974 *Z. Anorg. Allg. Chem.* **403** 1
[9] Cheetham A K, Fender B E F, Fuess H and Wright A F 1976 *Acta Crystallogr.* B **32** 94
[10] Maximov B and Schulz H 1985 *Acta Crystallogr.* B **41** 88
[11] Zalkin A and Templeton D H 1985 *Acta Crystallogr.* B **41** 91
[12] Belzner A, Schulz H and Heger G 1993 *Z. Kristallogr.* **209** 239
[13] Greis O, Ziel R, Breidenstein B, Haase A and Petzel T 1995 *Powder Diffract.* **10** 44
[14] Greis O and Cader M S R 1985 *Thermochim. Acta* **87** 145
[15] Sobolev B P, Fedorov P P, Seiranian K B and Tkachenko N L 1976 *J. Solid State Chem.* **17** 201
[16] Schlyter K 1952 *Ark. Kemi* **5** 73
[17] Sobolev B P, Ratnikova I D, Fedorov P P, Sinitsyn B V and Shahkalamyan G S 1976 *Mater. Res. Bull.* **11** 999
[18] Sobolev B P and Fedorov P P 1973 *Sov. Phys.–Crystallogr.* **18** 392
[19] Sobolev B P, Garashina L S, Fedorov P P, Tkachenko N L and Seiranyan K B 1974 *Sov. Phys.–Crystallogr.* **18** 473
[20] Jones D A and Shand W A 1968 *J. Cryst. Growth* **2** 361
[21] Oftedal I 1931 *Z. Phys. Chem.* **13** 190
[22] Spedding F H and Henderson D C 1971 *J. Chem. Phys.* **54** 2476
[23] Spedding F H, Beaudry B J, Henderson D C and Moorman J 1974 *J. Chem. Phys.* **60** 1578
[24] De Kozak A, Samouël M and Chrétien A 1973 *Revue Chim. Minér.* **10** 259
[25] Tanguy B, Portier J, Vlasse M and Pouchard M 1972 *Bull. Soc. Chim. Fr.* **3** 946
[26] Rotereau K, Gesland J Y, Daniel P and Bulou A 1993 *Mater. Res. Bull.* **28** 813
[27] Rietveld H M 1969 *J. Appl. Crystallogr.* **2** 65
[28] *Fullprof Program* 1992 Version 2.2 (written by J Rodriguez-Carvajal, CEA Saclay, France)
[29] Rotereau K, Daniel P and Gesland J Y 1998 *J. Phys. Chem. Solids* at press